Powder Technology 468 (2026) 121570

Contents lists available at ScienceDirect

Powder Technology

journal homepage: www.journals.elsevier.com/powder-technology

Impact of H_2-enrichment and ore mineralogy on the reduction of varying iron ores in suspension smelting ironmaking

Philipp Leerhoff [a,*], Johannes C. Brouwer [a], Christiaan Zeilstra [b], Koen Meijer [b], Jan van der Stel [b], Shoshan T. Abrahami [a], Neslihan Dogan [a], Yongxiang Yang [a]

[a] Department of Materials Science and Engineering, Delft University of Technology, Delft 2628 CD, the Netherlands
[b] Tata Steel, IJmuiden 1970 CA, the Netherlands

HIGHLIGHTS

- Higher H_2-levels accelerate and increase magnetite to wustite conversion.
- Gas diffusion through the product layer controls reaction at temperatures ≥1673 K.
- Goethite-rich iron ore fines achieve higher conversion than those without goethite.
- Water-gas shift reaction influences gas composition.

GRAPHICAL ABSTRACT

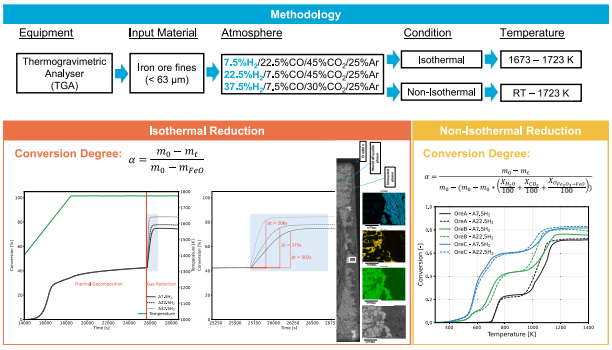

ARTICLE INFO

Keywords:
Hydrogen
Fine iron ore particles
Goethite
HIsarna® ironmaking
Water-gas shift reaction
Process metallurgy

ABSTRACT

Due to the high temperatures present in the HIsarna® process (~1773 K), the two reaction mechanisms thermal decomposition and gas reduction occur simultaneously during the pre-reduction of the injected iron ore fines. The objective of this study is to investigate the impact of H_2-enrichment in HIsarna reducing gas atmospheres on the pre-reduction of iron ores. Therefore, several iron ores, named OreA, OreB and OreC, with increasing amounts of goethite, were reduced by gas mixtures of H_2-CO-CO_2-Ar in a thermogravimetric analyser (TGA). A first approach studied the gas reduction as isolated process in isothermal conditions, whereas the second, non-isothermal approach, investigated thermal decomposition and gas reduction occurring simultaneously. In isothermal conditions the increase of H_2 in the atmosphere leads to an increase in conversion to wustite, and also to an increase in reaction speed. At 7.5 % H_2 in the atmosphere, the reaction saturates after 502–794 s, at 22.5 % H_2 after 375–583 s and at 37.5 % H_2 after 206–297 s, depending on the temperature. The reaction is controlled by the diffusion of the reducing gas through the developing product layer and the calculated activation energy is 77.60, 69.12 and 79.91 kJ/mol for H_2-contents of 7.5 %, 22.5 % and 37.5 %, respectively. In non-isothermal conditions, the influence of ore mineralogy is more significant compared to the H_2 increase in the atmosphere. An increase in total conversion is observed with an increase in goethite content in the ores.

* Corresponding author.
E-mail address: p.leerhoff@tudelft.nl (P. Leerhoff).

https://doi.org/10.1016/j.powtec.2025.121570
Received 8 April 2025; Received in revised form 13 August 2025; Accepted 18 August 2025
Available online 20 August 2025

1. Introduction

The iron- and steelmaking industry is responsible for 7–9 % of the global anthropogenic produced CO_2-emissions [1]. A radical change in production methods is necessary to reduce emissions and lead the steel industry into a more sustainable future. The biggest potential impact will be the substitution of the blast furnace, which is contributing to 71 % of the CO_2-emissions, globally arising from iron and steel production [2]. HIsarna® was developed by Tata Steel in IJmuiden as an alternative ironmaking process to the blast furnace [3]. HIsarna can be categorized as a smelting reduction process. Smelting reduction describes the combination of iron ore reduction and subsequent melting to liquid (pig) iron in a single reactor, without coke usage [4]. The most commercially established forms of smelting reduction are the COREX and FINEX processes, with COREX operating with a shaft furnace and FINEX with a multi-stage fluidized bed as the pre-reduction stage, before the material is melted for complete reduction [4]. However, further alternatives are under investigation.

A significant advantage of HIsarna compared to the blast furnace is that HIsarna accepts various raw materials as input material. In contrast to the blast furnace, HIsarna operates with un-coked coal and un-agglomerated iron ore fines, thereby combining the three process steps of ore agglomeration, coking, and ironmaking into a single process step [5]. The pilot scale of HIsarna already indicates that CO_2-emissions can be reduced by up to 20 % compared to the classic blast furnace process, and by at least 80 % in combination with carbon capture and storage (CCS) technology [4,6]. In HIsarna, the pre-reduction occurs in an upper cyclone converter before final reduction takes place in a lower molten bath, similar to the HIsmelt technology [7]. Initial reactions and pre-reduction occur very fast in the upper section of HIsarna. The ores are injected horizontally from the top-section of the furnace, where they immediately come into contact with the hot process gas arising from the lower section, which is a mixture of CO, CO_2, H_2, H_2O and N_2 [5]. The oxidation state and, therefore, the reduction capability of the off-gas arising from the smelting vessel is described by the post-combustion ratio (PCR) (equation (1)) [5].

$$PCR = \frac{\%H_2O + \%CO_2}{\%H_2O + \%CO_2 + \%H_2 + \%CO} * 100\% \quad (1)$$

The PCR is the lowest when the reducing gas reaches the pre-reduction section of the furnace. Following it reacts with the injected ores over the height of the furnace, until it is almost completely post-combusted at the top. The PCR value of the reducing gas entering the pre-reduction section of HIsarna is approximately 50–60 % while this value reaches 98 % when the gases are leaving the process [7,8]. This change is due to the decrease in concentration of H_2 and CO as iron ore particles are reduced and the partial combustion with oxygen. The behaviour of the PCR in the pre-reduction section of HIsarna is presented in Fig. 1. In this section of HIsarna, two main reaction mechanisms occur simultaneously. The first mechanism is the thermal decomposition of the injected ore particles, and a second is the gas-solid reduction with the reducing gases. From a thermodynamic perspective, the reduction of iron ore through thermal decomposition and gas reduction follows the same fundamental process that achieves the removal of oxygen from the ore.

HIsarna has the further advantage that it can accept untreated, lower-grade ores as input ores and is not limited to hematite and magnetite, which are categorized as high-grade ores (>65 % Fe [9]). Ores of interest for use in HIsarna are goethite ores, which are abundantly available in India [10]. Due to the lower iron content in the goethite phase (FeOOH) compared to the hematite phase (Fe_2O_3), an increase in goethite content in the ore would further decrease the grade of the ore. The influence of thermal decomposition on the reduction of various ores in HIsarna ironmaking has been studied in a previous publication [11], with a special focus on the impact of goethite content in the ores, and was based on preceding studies from Qu et al. [12] and Chen et al. [13]. The previous work related to goethite ores includes the kinetic analysis of goethite thermal decomposition as well as hematite thermal decomposition and investigates the influence of goethite content and further ore mineralogy on the overall reduction.

To complete this preceding research, the current study focuses on the mechanism of gas reduction and its influence on the reduction kinetics in smelting reduction processes, especially under HIsarna ironmaking conditions. Currently, HIsarna exhibits pre-reduction degrees of 20–25 % in its upper section [7]. Due to its nature, HIsarna is limited to the use of CO-CO_2-H_2-H_2O gas mixtures as reducing gases. However, it is generally known that hydrogen enhances the reaction kinetics of iron ore reduction [14]. Therefore, this study aims to investigate the influence of increasing hydrogen levels in HIsarna reducing gas mixtures on the reduction degree and kinetics.

The reduction of iron oxides in isothermal conditions has been intensely studied in literature [15–22]. Zuo et al. [17] studied the

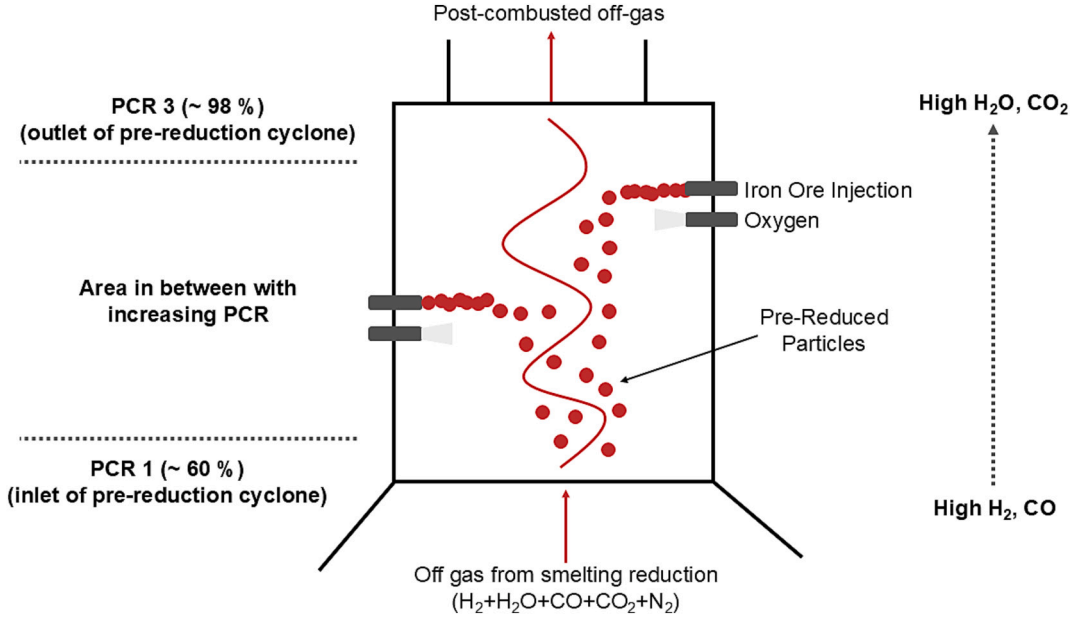

Fig. 1. Schematic of HIsarna pre-reduction section, adapted from [8].

reduction of hematite pellets in several H_2-CO mixtures at 1073, 1173 and 1273 K and found a positive effect of hydrogen enrichment in the atmosphere on the speed of the reduction, explained by the enhanced diffusivity of the reducing gas through the sample. Therefore, it is critical to better understand the impact of hydrogen on the mechanisms of gas reduction. Sohn et al. [16] studied the reduction of hematite pellets to metallic iron with hydrogen in a temperature range of 973 to 1173 K and found the reaction to be initially controlled by a topo-chemical reaction, forming in initial iron layer, before the rate-limiting mechanism shifts to pore diffusion in the later stages.

Next to the reaction mechanism, determining the activation energy is crucial to evaluate the influence of hydrogen enrichment on the reduction. Even though many studies have been carried out, insights vary considering the influence of H_2 and CO levels in the reducing gas on the activation energy. Zhang et al. [15] studied the conversion of New Zealand ironsand pellets and Sohn et.al [16] of metal doped hematite pellets to metallic iron with pure hydrogen. Zhang et al. calculated an activation energy of 31.3 kJ/mol, whereas Sohn et al. calculated activation energies between 15 and 29 kJ/mol depending on the reduction step. Also, Moon et al. [18] studied the reaction kinetics of varying H_2-CO reducing gas mixtures and determined activation energies between 19.8 and 42.1 kJ/mol, where the values decreased with an increase in CO content. Piotrowski et al. [23] tried to find differences between the influence of CO and H_2 as reducing gases by testing mixtures of 90 % N_2 with either 10 % H_2, CO or H_2 + CO for the conversion of hematite powder into wustite. Even though the three mixtures have the same ratio of reducing gases, the arising activation energy differs strongly. The mixture containing only CO as reducing gas showed the highest activation energy (122.52 kJ/mol), followed by the mixture containing CO and H_2 (93.72 kJ/mol) and the mixture containing only H_2 showed by far the lowest activation energy (28.08 kJ/mol).

Considering the kinetic data, multiple parameters can influence the reduction mechanism and resulting activation energy: material properties, reducing gas atmosphere, the considered reduction step and many more [24], underlining the need for continuous research. Most studies, however, are focusing on the adaptation of hydrogen in temperature ranges which are more in relation to the direct-reduced iron (DRI) production conditions, which typically operate below 1273 K [4] and are therefore focusing on significantly lower temperatures then the gas-solid reduction in the HIsarna pre-reduction section (T ~ 1773 K [8]). The thermal decomposition of goethite and hematite as well as the reduction of hematite with reducing gases, containing H_2 and CO in non-isothermal conditions have also been significantly studied in literature [11,13,25–32]. However, these studies either focused on a single iron-bearing phase being reduced, or, when examining samples containing hematite and goethite, inert atmospheres were applied to only observe the thermal decomposition. This leaves the question open on how a mixed system of goethite and hematite would reduce in non-isothermal conditions with the two mechanisms thermal decomposition and gas reduction happening simultaneously. The influence of goethite content and further mineralogy on the reduction behaviour in hydrogen enriched HIsarna atmospheres requires further study, since it is important to understand the influence of a complex ore mineralogy on the overall reduction behaviour, particularly at temperatures greater than 1273 K.

To summarize, the objective of this experimental study is to gain a complete overview of the reduction behaviour and kinetics of the ores in the utilized gas atmospheres under HIsarna process operating conditions. Since the thermal decomposition behaviour of the ores has been discussed previously in [11], this study is meant to provide insight into gas reduction as an isolated (isothermal approach) and co-occurring (non-isothermal approach) process with thermal decomposition. Focus is placed on the influence of ore mineralogy, hydrogen enrichment in the reducing gas atmosphere, and a potential decrease in PCR on the reducibility and reduction mechanisms of the varying iron ores.

2. Method

2.1. Materials

The three iron-bearing ores, named OreA, OreB and OreC, with a particle size <63 μm were provided by Tata Steel. To gain insight into the differences in chemical composition and mineralogy between the ores, X-ray diffraction (XRD), X-ray fluorescence (XRF) and loss of ignition (LOI) analyses were conducted. XRD analysis was carried out with a Bruker D8 Advance diffractometer Bragg-Brentano geometry and Lynxeye position sensitive detector (Bruker Germany). The main mineralogical phases, according to XRD, for OreA are hematite (Fe_2O_3), quartz (SiO_2) and dolomite ($CaMg(CO_3)_2$, with small amounts of magnetite (Fe_3O_4). The main difference of OreB and OreC compared to OreA is the presence of the goethite phase. For OreB, the main phases, in addition to hematite and goethite, are quartz and kaolinite ($Al_2Si_2O_5(OH)_4$). The XRD of OreC measured only quartz as non-iron-bearing phase, next to hematite and goethite. Due to the complex chemical composition of the ores, the XRD signals show many smaller peaks, indicating additional gangue materials that cannot be accurately identified. The detailed XRD results are displayed in Fig.S1 in the supplementary materials.

The elemental composition of the ores was obtained by XRF (Panalytical AXIOS XRF, Netherlands) and LOI analysis (dissolution in nitric acid and TGA (LECO, Germany) and is summarized in Table 1. All three ores used in this study can be categorized as low-grade ores (< 62 % Fe [9]), with OreB showing the highest amounts of total iron (61.60 wt.-%) and OreC the lowest (56.80 wt.-%). In alignment with the XRD analysis, SiO_2 and Al_2O_3, are found to be the main gangue components in all three ores. OreB contains the highest amounts of Al_2O_3, while OreC contains the highest SiO_2 content. In contrast to OreB and OreC, OreA contains larger amounts of CaO and MgO due to the presence of a dolomite phase. The crystal water present in OreB and OreC indicate the goethite phase, which is absent in OreA. Considering the difference in crystal water between OreB (2.19 wt.-%) and OreC (6.05 wt.-%), the amount of goethite in OreC is expected to be substantially higher.

A deeper analysis of the input materials can be found in the preceding study [11], where differences in morphology, phase and impurity distribution and general mineralogy of the materials are explained in detail.

2.2. Experimental approach

To obtain insights into the topo-chemical reduction behaviour of the varying iron ores and the reaction kinetics under non-isothermal and isothermal conditions, high temperature experiments were carried out under three different reduction conditions. The operating parameters are detailed in Table 2. In order to mimic the gas composition of HIsarna, a main PCR of 60 % was chosen. A total flow rate of 200 ml/min was

Table 1
Chemical composition of OreA, OreB and OreC, determined by XRF and LOI after normalization.

		OreA	OreB	OreC
	Fraction [μm]	< 63	< 63	< 63
Compound	Fe_2O_3	85.93	88.07	81.21
	total-Fe	60.10	61.60	56.80
	SiO_2	5.18	4.96	6.84
	Al_2O_3	2.24	3.81	3.52
	MgO	0.71	0.04	0.14
	CaO	1.99	0.05	0.11
[wt.-%]	TiO_2	1.04	0.33	0.18
	MnO	1.20	0.03	1.07
	CO_2 (carbonate)	1.52	0.21	0.65
	H_2O(crystal)	–	2.19	6.05
	Rest	0.37	0.25	0.26

Table 2
Experimental conditions in TGA, Setaram TAG 16/18.

Experimental Condition	Operating Parameter
Ore isothermal conditions	B
Ore non-isothermal conditions	A, B, C
Holding time non-isothermal conditions (h)	2
Holding time isothermal conditions (h)	2 + 1
Heating rate (K/min)	5
Particle size (μm)	< 63
Temperature (K)	298–1773
Flow rate	200 ml/min
Reducing atmosphere (vol-%)	A7.5H_2 (PCR = 60 %): 7.5 %H_2/22.5 %CO/45 %CO_2/25 %Ar A22.5H_2 (PCR = 60 %): 22.5 %H_2/7.5 %CO/45 %CO_2/25 %Ar A37.5H_2 (PCR = 40 %): 37.5 %H_2/7.5 %CO/30 %CO_2/25 %Ar

applied. Of that 200 ml/min, 50 ml/min was always argon, necessary as a shielding gas for the thermo-couples. The remaining 150 ml/min reflects the reducing gas composition. A decrease in PCR value would provide the option of higher hydrogen contents in the reducing gas. Two different atmospheres (A7.5H_2 & A22.5H_2) were selected to evaluate the influence of hydrogen enrichment in an atmosphere with a PCR of 60 % on the reduction of the varying ores. To evaluate the influence of a lower PCR, a third atmosphere based on a PCR = 40 % (A37.5H_2) with the same total flow rate was tested. The experiments were conducted in a symmetrical thermogravimetric analyser (TGA, Setaram TAG 16/18, Caluire, France). Alsint crucibles with an inner diameter of 10 mm, a height of 20 mm, and a wall thickness of 2 mm were used as sample holders. A material amount of 300 mg was used as input.

In the non-isothermal approach, the ore particles were gradually heated in the reducing gas atmosphere at a heating rate of 5 K/min until a temperature of 1773 K was reached. After 1773 K was reached, a holding time of 2 h was applied to observe the behaviour of the reducing gas at elevated temperatures and to achieve the reduction limit. In the isothermal approach, the ores were gradually heated in an argon atmosphere at a heating rate of 5 K/min until a set temperature of 1673 K, 1723 K or 1773 K was reached. After the set temperature was reached, the material was held isothermally at that temperature for 2 h under an argon atmosphere to reach the limits of thermal decomposition. After 2 h, reducing gases were introduced for 1 h to observe the reduction kinetics under isothermal conditions. This approach enables the observation of gas reduction as an isolated phenomenon, considering that the thermal decomposition process had been completed earlier. The experiments under isothermal conditions were only carried out on OreB. In both tests, the material was cooled to room temperature in the system under an argon atmosphere at a controlled cooling rate of 5 K/min. The mass loss was measured as the primary output, either over increasing temperature at a constant heating rate (non-isothermal conditions) or over increasing time at a constant temperature (isothermal conditions), to analyse the reduction kinetics of the process.

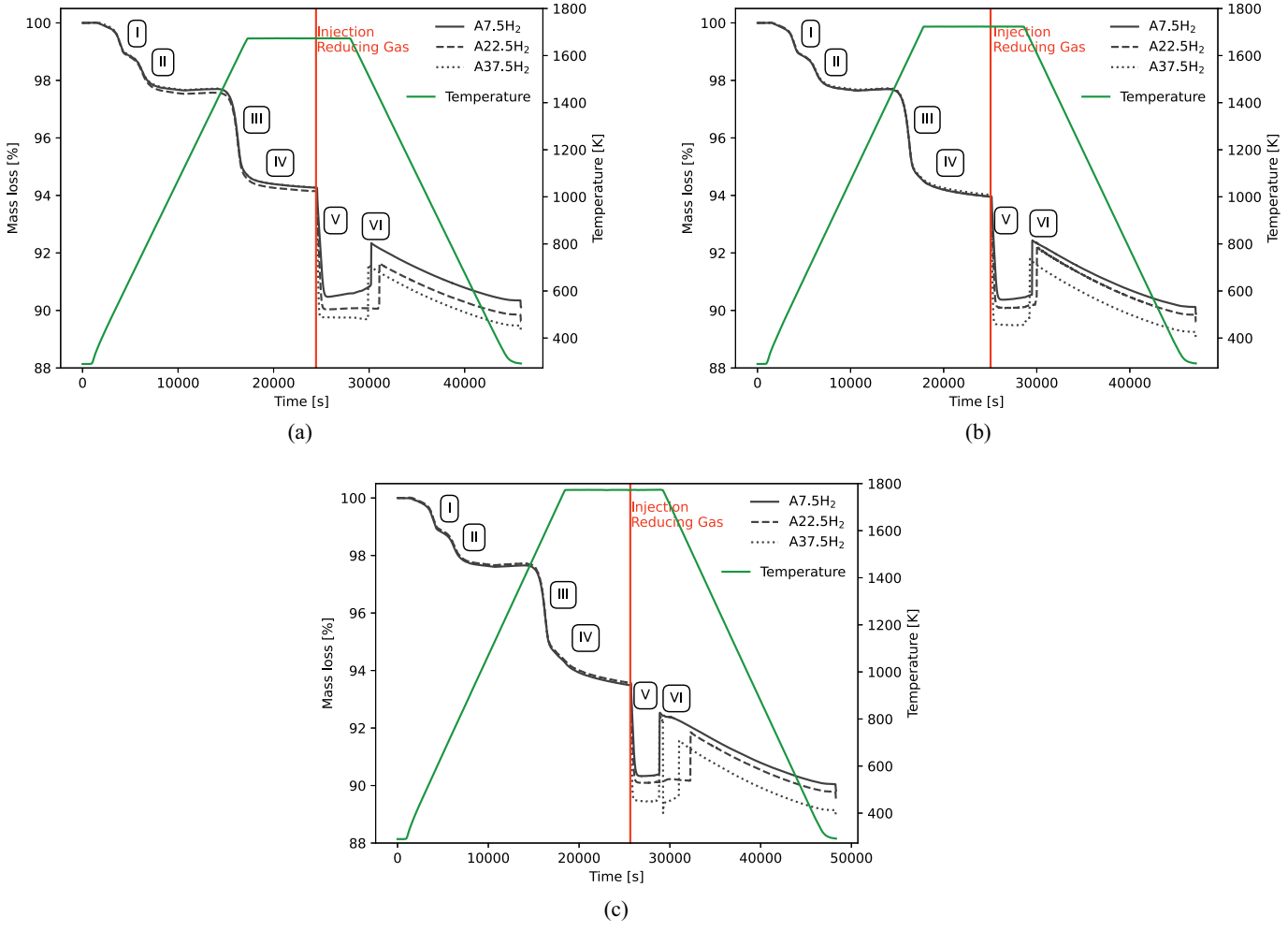

Fig. 2. Mass loss over time with respect to reduction atmosphere for isothermal TGA experiments of OreB at (a) T = 1673 K, (b) T = 1723 K and (c) T = 1773 K.

3. Results and discussion

3.1. Isothermal reduction

Fig. 2 depicts the general mass loss of the isothermal experiments for OreB. The red line in the figure marks the start of the reducing gas injection while the green line shows the temperature profile over time. In general, six distinct stages can be observed. The first four stages are all part of the thermal decomposition of the ore, occurring before the reducing gas is injected. These stages were identified in our previous publication [11]. The first two stages were assigned to goethite decomposition, while stages three and four were assigned to the thermal decomposition of hematite. In this study, stages five and six are of interest, since these depict the reduction of the decomposed material with the defined reducing gas mixture. A sharp mass loss is observed directly after the injection of the reducing gas (V). The mass losses achieved in this stage are 3.8 %, 4.1 % and 4.5 % at 1673 K, 3.6 %, 3.8 % and 4.5 % at 1723 K and 3.2 %, 3.5 % and 4.1 % at 1773 K, for A7.5H_2, A22.5H_2 and A37.5H_2, respectively. At all temperatures, the mass loss increases with increasing hydrogen content in the atmosphere. The mass loss in stage five decreases with increasing temperature due to the higher mass loss already achieved through thermal decomposition at higher temperatures. Following this initial decrease, the mass loss remains constant for a period. At later stages of the isotherm, an increase in mass is observed. This phenomenon is related to pressure changes in the system caused by the water-gas shift reaction taking place. The reactions occurring and their influence on the system will be discussed in more detail in the section 3.4..

3.2. Isothermal reduction kinetics

The essential characteristic parameter for the kinetic models used in this study is the conversion factor α (equation (2)).

$$\alpha = \frac{m_0 - m_t}{m_0 - m_a} \tag{2}$$

Where m_0 is the mass of the initial sample (mg), m_t is the mass of the sample at time t (mg) and m_a is the mass of the sample after complete conversion (mg). Due to thermodynamic and kinetic limitations, the formation of metallic iron is not expected under the studied conditions. Therefore, wustite (FeO) is considered the final reduction product, meaning that a conversion factor of 1 corresponds to the complete conversion of hematite to wustite. The conversion degree (equation (2)) is calculated based on the conversion of hematite (Fe_2O_3) to wustite (FeO) over the whole reaction range. After thermal decomposition (stages I-IV), it is expected that mostly magnetite is present as the iron bearing phase. However, to avoid assuming that only magnetite is present before the gas reduction, the conversion factor is defined over the entire reaction range, including thermal decomposition, as presented in Fig. 3. The images show the calculated conversion factors for OreB at three temperatures and the respective atmospheres. The conversion of hematite to magnetite by thermal decomposition initiates around 1419 K, which also depicts the start of the figure. All reactions occurring before that temperature do not contribute to the calculated conversion degree.

At all temperatures, similar trends are seen for all three atmospheres after the reducing gases are introduced to the system (as indicated by the red line in Fig. 3). Considering A7.5H_2 and A22.5H_2, an increase in H_2 content at the same PCR leads to a higher total conversion. At 1673 K the conversion degree increases from approximately 73.5 to 77 %, at 1723 K from 74.7 to 78 % and at 1773 K from 74.8 to 78 %. This further shows that there is no strong influence of the holding temperature on the total conversion. A decrease in PCR, and therefore an increase in reducing gas content, leads to an even higher total conversion during the gas reduction phase. The total conversion reached in A37.5H_2 at 1673 K is around 81.3 %, at 1723 K 84 % and at 1773 K 84 %. As comparison, the conversion factors at equilibrium for each atmosphere and temperature were calculated using FactSage 7.0 [33] (FactPS database) [34] and were determined to vary between 96 % and 103 %, depending on atmosphere and temperature. It can be noted that for all experimental conditions, complete conversion is never reached, indicating kinetic limitations for the gas reduction.

Fig. 3 also highlights the strong influence of the atmosphere on the steepness of conversion during the gas reduction. To better visualize this influence, Fig. 3 includes a zoomed-in view of the main area of gas reduction until the experimental equilibrium is reached ((a2), (b2), (c2)). Overall, the influence of hydrogen content is much stronger compared to the temperature influence. Even though higher temperatures always lead to faster reduction in the respective atmosphere, it cannot always compensate for the influence of increasing hydrogen levels. The increase in hydrogen level from A7.5H_2 to A22.5H_2 leads to a decrease in reduction time from 502–794 s to 375–583 s, depending on the temperature. A further change to lower PCR and even higher hydrogen levels in A37.5H_2 decreases the reduction times further to 206–297 s.

In order to get a more detailed overview of the reduction achieved in the separate thermal decomposition and gas reduction stages, the calculated conversion degrees (Fe_2O_3 → FeO) for each stage are presented in Table 3. A small variation in the conversion after thermal decomposition (α_{TD}) is seen based on the set temperature. With an increase in temperature, slightly higher conversion, with a minimum of 35.2 % at 1673 K and a maximum of 42.6 % at 1773 K, is achieved during thermal decomposition. Further, it is observable that the influence of the atmosphere on the final conversion (α_{final}) is stronger than the influence of the temperature. For all temperatures, a final conversion of around 73 % is reached for A7.5H_2, around 75–76 % for A22.5H_2 and around 80–82 % for A37.5H_2, after 1 h reduction. Considering only the conversion achieved during gas reduction, α_{GR} increases from 37.3 % to 44.6 % at 1673 K, from 34.7 % to 43.8 % at 1723 K, and from 29.9 % to 38.7 % at 1773 K with increasing H_2 content in the reducing gas. The decrease in α_{GR} with increasing temperature is explained by the higher degree of reduction already achieved during thermal decomposition at higher temperatures.

In the next step, the reaction mechanism as well as the kinetic parameters of the isothermal experiments were determined. A common model used to explain reaction kinetics in ironmaking is the (un-)reacted shrinking core model (USCM) [35]. Based on the shrinking core model, the reaction first takes place at the outer skin of a particle, creating a stable product layer. The reaction front then moves inwards, shrinking the unreacted core of the particle [35]. Normally, the shrinking core model assumes spherical particles. However, Luo and Wu [36] found that the shrinking core model is still applicable for an aspect ratio of $0 < h/2r < 1$, where h is the height and r the radius of the sample. In this study, the whole sample in the crucible was considered and the aspect ratio of the studied samples is approximately ~0.12. The authors assumed that the shrinking core model is applicable in this study. The reacting and shrinking of the core occur step-wise [35]. The reaction steps used to determine the mechanisms of the reductions in this study are the internal pore diffusion, chemical reaction, and the mixed mechanism of the two. The reaction rate constants can be derived based on the proposed reaction mechanisms using the following mathematical formulations [37–39]:

Internal Diffusion Control:

$$1 - \frac{2}{3}\alpha - (1-\alpha)^{\frac{2}{3}} = kt = \frac{6D_e(C_0 - C_e)}{\rho_0 r_0^2}t \tag{3}$$

Interface Chemical Reaction Control:

$$1 - (1-\alpha)^{\frac{1}{3}} = kt = \frac{k(1+K_e)(C_0 - C_e)}{K_e r_0 \rho_0}t \tag{4}$$

Mixed Control:

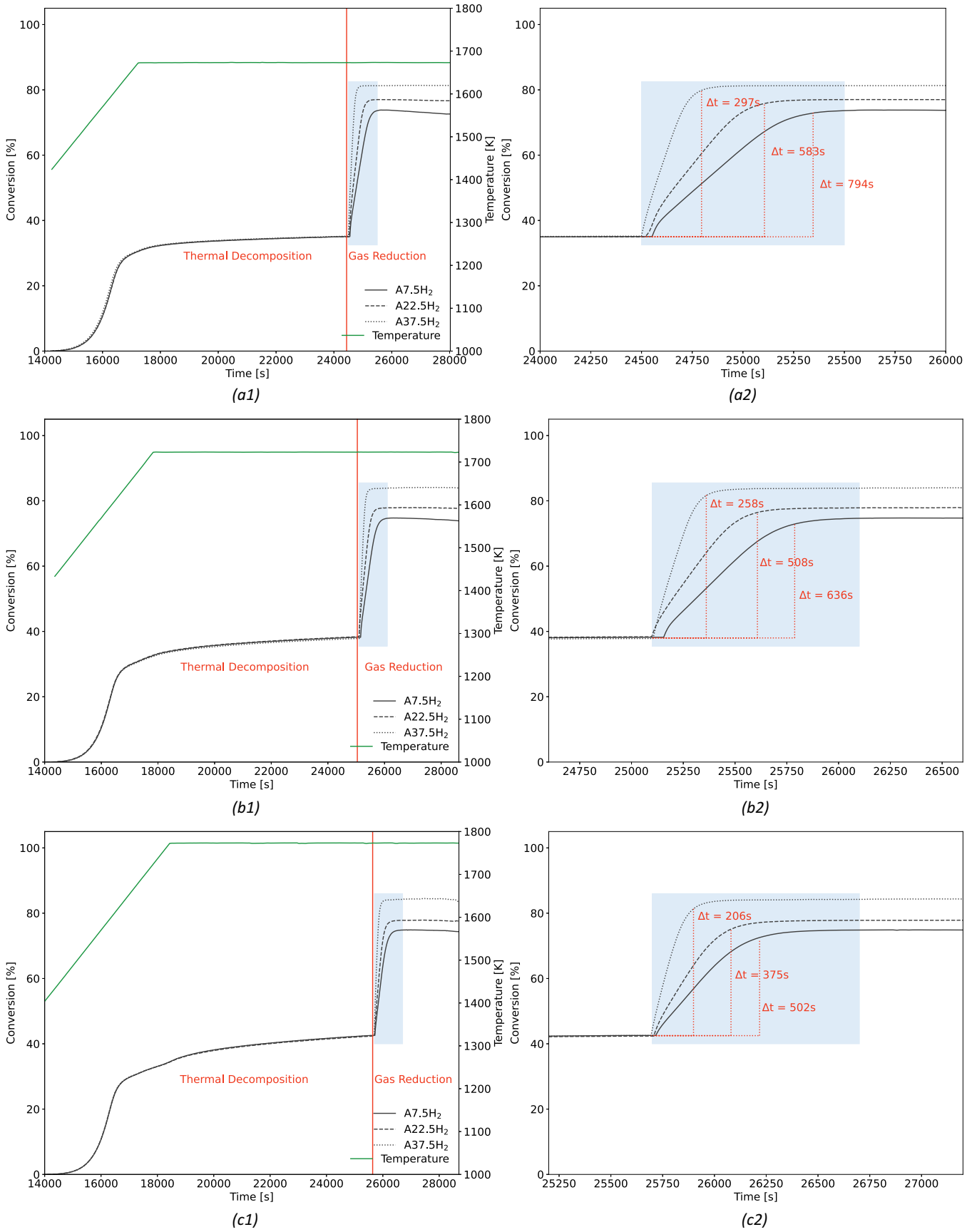

Fig. 3. Conversion factor for thermal decomposition and gas reduction of OreB at (a1) $T = 1673$ K, (a2) 1673 K zoomed-in, (b1) $T = 1723$ K, (b2) 1723 K zoomed-in and (c1) $T = 1773$ K, (c2) 1773 K zoomed-in.

Table 3
Conversion degrees after thermal decomposition (TD) and after gas reduction (GR) of OreB.

	1673 K			1723 K			1773 K		
	$A7.5H_2$	$A22.5H_2$	$A37.5H_2$	$A7.5H_2$	$A22.5H_2$	$A37.5H_2$	$A7.5H_2$	$A22.5H_2$	$A37.5H_2$
α_{TD} [%]	35.6	35.4	35.2	38.2	39	37.8	42.6	42.4	42.6
α_{Total} [%]	72.9	75.8	79.8	72.9	76.4	81.6	72.5	75.1	81.31
α_{GR} [%]	37.3	40.4	44.6	34.7	37.4	43.8	29.9	32.7	38.7

$$\frac{t}{1-(1-\alpha)^{\frac{1}{3}}}=\frac{\rho_0 r_0^2}{6D_e(C_0-C_e)}\left[1+(1-\alpha)^{\frac{1}{3}}-2(1-\alpha)^{\frac{2}{3}}\right]+\frac{\rho_0 r_0 K_e}{k(1+K_e)(C_0-C_e)} \quad (5)$$

where α is the conversion factor of hematite to wustite (−), k is the reaction rate constant (s^{-1}), t is the time (s), D_e is the diffusion coefficient of the reducing gas into the product layer (m^2/s), C_0 is the reducing gas concentration at the surface (mol/m^3) and C_e in equilibrium (mol/m^3), ρ_0 is the initial oxygen density (mol/m^3), r_0 is the initial radius (m) and K_e is the equilibrium constant (−).

By plotting $1-(1-\alpha)^{\frac{1}{3}}$ *vs.* t (Chemical Reaction), $1-\frac{2}{3}\alpha-(1-\alpha)^{\frac{2}{3}}$ *vs.* t (Diffusion) and $\frac{t}{1-(1-\alpha)^{\frac{1}{3}}}$ *vs.* $1+(1-\alpha)^{\frac{1}{3}}-2(1-\alpha)^{2/3}$ (Mixed), the reaction mechanism can be determined based on the best fitting of the model. The reaction rate constant k can be obtained from the slope of the plot. The fitting results of the three mathematical models are presented in Table 4.

It can be seen that the fitting of the mixed controlled model is the poorest, whereas the R^2 of the interface chemical reaction control and internal diffusion are all >0.99 and can therefore represent the

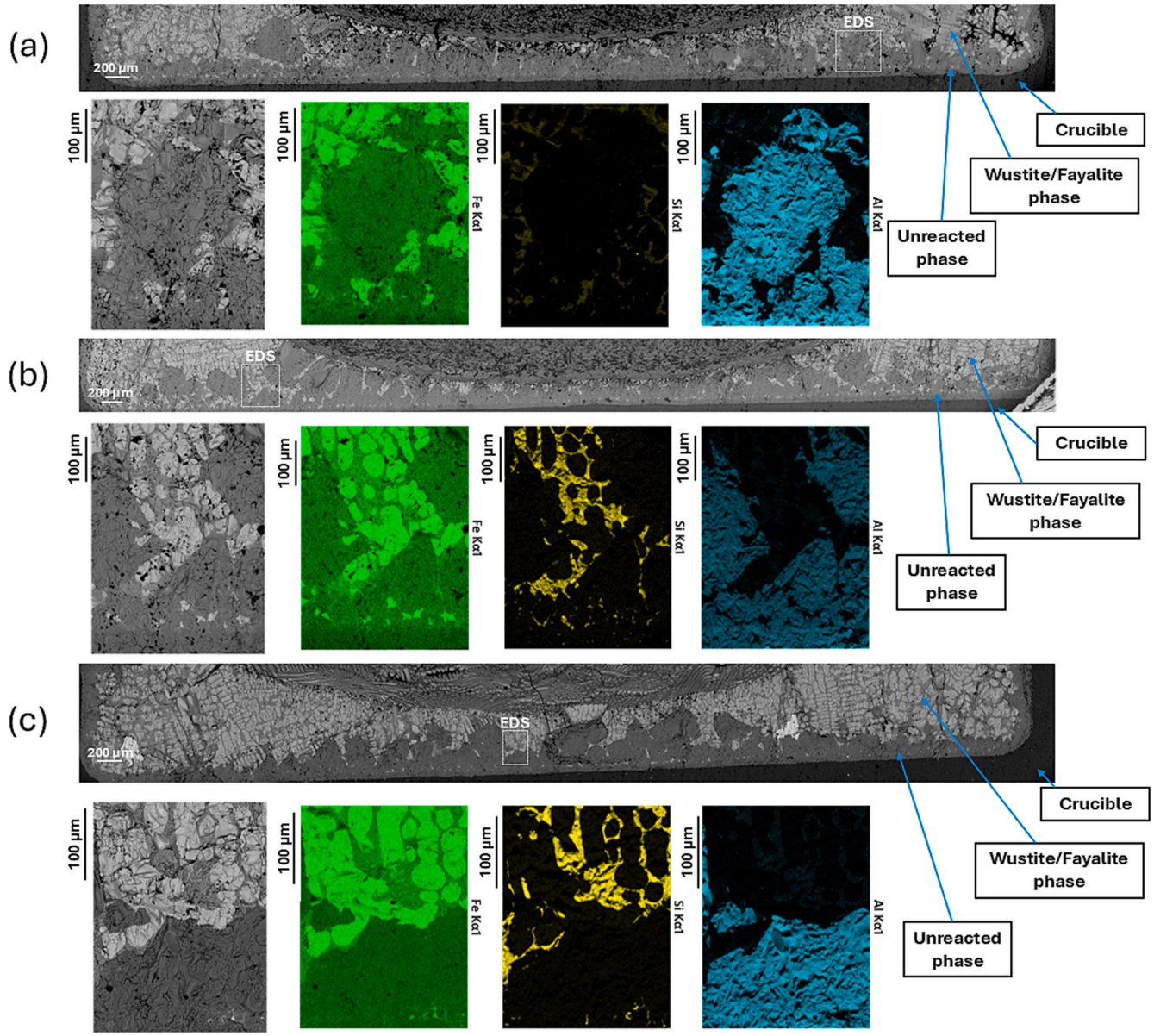

Fig. 4. Results of SEM-EDS of a cross section of OreB sample under (a) $A7.5H_2$, (b) $A22.5H_2$ and (c) $A37.5H_2$ reducing atmospheres at 1773 K.

experimental data very well. Even though the fitting is slightly better for the internal diffusion control, it is difficult to determine the best model relying only on the model fit, due to their close proximity. To further identify the reduction mechanism, SEM imaging combined with electron backscattering and EDS measurements was carried out. The imaging visualizes the distribution of phases and elements through the material. Therefore, a cross-section of the sample, solidified in the crucible from experiments with the three atmospheres A7.5H_2, A22.5H_2 and A37.5H_2, reduced at a temperature of 1773 K, was sanded and polished. The imaging of each sample cross-section in combination with the mapping of the EDS analysis is presented in Fig. 4.

The results of the backscattering measurement clearly illustrate the presence of different phases in the solidified sample. The area with brighter contrast is expected to be richer in wustite, and the darker area in magnetite, due to the higher amount of iron in wustite. The EDS measurements further confirm this statement. Comparing the brighter color of the backscattering with the EDS results, higher iron content is measured in these areas. Furthermore, the distribution of silicon indicates that silicate mostly settles around areas of higher iron content. This indicates the formation of fayalite slag around areas of wustite. Fayalite (2FeO*SiO_2) is a common slag-phase arising in the converter process of copper production based on the reaction of wustite with silica (equation (6)) [4].

$$2FeO(l) + SiO_2(s) = 2FeO \bullet SiO_2(l) \quad (6)$$

FactSage 7.0 [33,34] calculations were carried out to evaluate the possible presence of the fayalite slag. Therefore, the final products of the thermal decomposition at the set-temperatures 1673, 1723 and 1773 K were calculated based on the chemical composition of OreB (Table 1). At the end of thermal decomposition, magnetite was the final iron-bearing phase and no fayalite slag was determined in the calculations. Next, the phases calculated at the end of thermal decomposition were used as input for the thermodynamic evaluation of the products arising during the isothermal gas reduction at the respective temperatures for A7.5H_2, A22.5H_2 and A37.5H_2. In these calculations three main phases were detected, which account for over 98 % of the total composition. For all three atmospheres and temperatures, approximately 73 % of the phase composition was wustite, 18–19 % fayalite and around 7 % hercynite ($FeAl_2O_4$). The theoretical evaluation of fayalite presencesupports the EDS findings of fayalite formation around the wustite phase. The EDS images further indicate lower amounts of aluminum around the wustite phase, which could potentially be the hercynite phase which is present in lower amounts based on the thermodynamic calculations. Other aluminum oxides are expected to stay unreacted during the reduction, probably even solid. The distribution of alumina shows that it settles at the bottom of the crucible, in the area of lower iron content. The imaging shows a strong reduction on the surface of the sample, forming a reduced product layer. The reduction further proceeds (un-uniformly) throughout the sample. This behaviour indicates that the reduction of the sample is not limited by the chemical reaction at the interface, but by the internal diffusion of the reducing gases. Based on these microscopical findings and the model fit, internal diffusion is assumed to be the rate-limiting mechanism. Sohn et.al [16] determined the reaction mechanism of hematite with hydrogen to be of mixed control, with the reaction rate to be initially governed by a topochemical reaction forming an initial iron layer (5–80 s), and following shifting to pore diffusion (119–671 s) after the product layer was formed. This second mechanism, which is responsible for most of the reduction time, is similar to the diffusion control found in this study. Considering the higher reaction temperatures in this study (1673 K – 1773 K) compared to Sohn et al. (973 K – 1173 K), it is possible that the initial formation of the product layer is occurring faster, making it difficult to distinguish between the two mechanisms, resulting in internal diffusion emerging as the overall rate defining mechanism. This is also underlined by the bad results of the model fitting for the mixed control in Table 4.

Based on this model choice, the reaction rate constant was calculated and is presented in Fig. 5a. Considering the reaction rate constant, k, a coherent increase with hydrogen content and temperature is observable, indicating a more efficient diffusion process at higher H_2 levels. Overall, the chemical reaction is more sensitive to the temperature compared to physical mechanisms like diffusion [35]. Therefore, the impact of the increasing H_2-levels in the atmosphere on the rate constant is much stronger than the influence of temperature, further supporting internal pore diffusion as the dominant mechanism compared to chemical reaction. The rate constants determined by Sohn et al. [16] are slightly higher compared to our study (lnk ~ −6.2 to −5.2), which can be explained by the use of pure hydrogen increasing the reaction rate. A significant increase in reaction rate constant occurs, comparing A37.5H_2 to A7.5H_2 and A22.5H_2, which can be explained by the decrease in PCR and therefore a greater presence of reducing gases, facilitating the reduction process.

Table 4
Results of model fitting with shrinking core model.

Atmosphere	Temperature [K]	R^2 (Mixed)	R^2 (Chemical Reaction)	R^2 (Diffusion)
A7.5H_2	1673	0.9246	0.9936	0.9940
	1723	0.9360	0.9957	0.9959
	1773	0.9416	0.9932	0.9965
A22.5H_2	1673	0.8939	0.9928	0.9957
	1723	0.9187	0.9925	0.9951
	1773	0.9315	0.9938	0.9975
A37.5H_2	1673	0.8892	0.9913	0.9931
	1723	0.9071	0.9952	0.9944
	1773	0.9146	0.9932	0.9963

The general expression for the reaction rate of the thermal decomposition process is presented in equation (7). Applying the Arrhenius equation, the expression for the reaction rate constant is obtained through equation (8).

$$\frac{d\alpha}{dt} = kf(\alpha) \quad (7)$$

$$k(T) = Aexp\left(-\frac{E_a}{RT}\right) \quad (8)$$

To obtain the activation energies for the varying atmospheres, Arrhenius fitting (equation (8)) was carried out and the results are presented in Fig. 5b. In this study, the important influence on the activation energy under isothermal conditions is the increase in hydrogen content in the reducing gas.

Considering A7.5H_2 and A22.5H_2, an increase in hydrogen content in the reducing gas leads to a decrease in activation energy from 77.60 to 69.12 kJ/mol. This is in alignment with the assumed diffusion model, considering the better diffusion ability of hydrogen compared to carbon monoxide, lowering the activation energy of A22.5H_2 compared to A7.5H_2 due to the shift from CO to H_2 as a dominant reducing gas. Bahgat et al. [40] observed the reduction of magnetite single crystals with hydrogen in a TGA at 1173–1373 K. Considering the reduction step of Fe_3O_4 to Fe, they concluded a solid state diffusion as the reduction mechanism, explained by wustite phases entrapped in dense metallic iron, and calculated an activation energy of 99.2 kJ/mol This value is significantly higher compared to our study. The lower activation energies in our study can be explained by the higher temperatures applied and the lower achieved conversion degree. Based on the decrease in activation energy between A7.5H_2 and A22.5H_2, a logical conclusion would be a further decrease in activation energy for A37.5H_2, due to the higher amounts of hydrogen in the atmosphere. However, in this case, the activation energy increases to 79.91 kJ/mol, indicating kinetic limitations in this reaction. An explanation for this could be the higher achieved conversion in A37.5H_2. Despite the presence of more hydrogen in the atmosphere leading to a faster reaction, increasing the reaction rate constant, the push to a higher conversion degree could require more

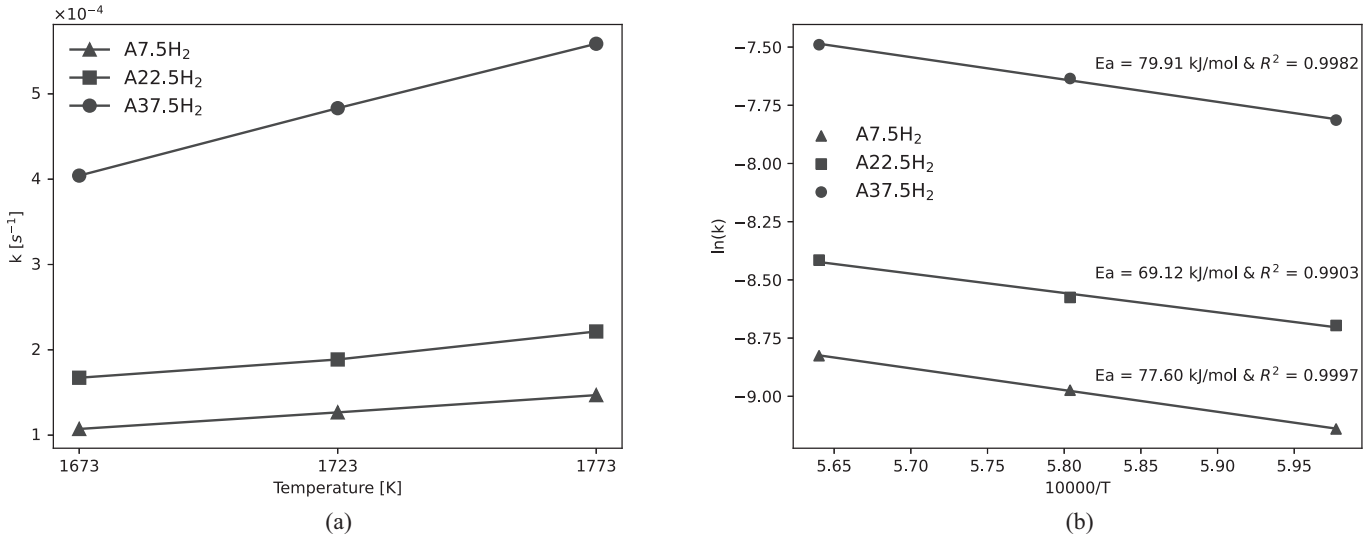

Fig. 5. (a) Reaction rate constant based on diffusion as the rate-limiting step and (b) resulting Arrhenius fitting.

energy and therefore increases the overall activation energy for the reaction. Even though Hammam et al. [28] determined a decrease in activation energy with increasing conversion during hematite reduction by hydrogen, Chen et al. [41] found the activation energy to increase with increasing conversion in a gas mixture of CO-N_2, where the highest activation energy was found to be 47.14 kJ/mol for a conversion range of 20 to 90 %.

Considering the influence of H_2 and CO levels in the reducing gas on the activation energy, insights vary between studies. Zhang et al. [15] determined an activation energy of 31.3 kJ/mol and Sohn et.al [16] of 17.52–20.01 kJ/mol at a conversion degree of 20 % and 14.81–20.50 kJ/mol at a conversion degree of 40 % for the reduction of hematite pellets to metallic iron with hydrogen. Moon et al. [18] calculated the activation energy to vary between 19.8 and 42.1 kJ/mol for different mixtures of H_2 and CO, with the highest activation energy determined for pure H_2 and the lowest for pure CO. These activation energies are lower compared to our study. The main difference is that our study applies gas mixtures containing oxidizing gases (CO_2), which limit the reduction and therefore increase the activation energy. The influence of H_2 and CO in the reducing gas on the conversion of hematite to wustite was also studied by Piotrowski et al. [23]. For a gas mixture of 90 % N_2 and 10 % CO, they found an activation energy of 122.52 kJ/mol. When the 10 % CO was exchanged with 5.7 % CO and 4.3 % H_2, the activation energy decreased to 93.72 kJ/mol. A further shift to a gas mixture of 90 % N_2 and 10 % H_2 significantly decreased the activation energy to 28.08 kJ/mol. Even though they described the initial reaction as topochemical surface control, the reaction mechanism changed to diffusion control after an initial layer of Fe_3O_4/FeO formed, which is again in alignment with the mechanism determined in this study. Dilmac [30] used fine hematite ore as input material and CO-N_2 atmospheres (50 % CO) as reducing gas. Even though they investigated multiple reduction steps, the important step to compare to this study is the reduction from magnetite to wustite. The model fitting of Dilmac led to a reaction mechanism of two-dimension contraction and an activation energy of 54.93 kJ/mol for the reduction of magnetite to wustite.

In summary, research on the reduction of iron ores by varying reducing gas composition may be vast but differs strongly due to the various parameters influencing the reduction kinetics. It should be noted that the reduction temperatures in this study are significantly higher than in the studies mentioned above. However, the activation energies calculated in this study based on the internal diffusion model (69.12–79.91 kJ/mol) fit the trends in literature. While studies using pure H_2 generally show lower activation energies, the activation energies in our study are higher due to the presence of Ar and CO_2. Studies with larger amounts of nitrogen or lower reducing gas contents come closer to or exceed the kinetic parameters in this study.

3.3. Non-isothermal reduction

During the reduction under non-isothermal conditions, gas-solid reduction occurs together with thermal decomposition as co-existing processes. In our previous study [11], the thermal decomposition behaviour of three ores (OreA, OreB, OreC) was studied and significant differences in mass loss were explained by the mineralogical differences of the ores. Two different decomposition processes were identified for each ore. OreA first shows the decomposition of the dolomite phase, before hematite decomposes as a two-stage process. OreB and OreC first show the decomposition of goethite as two-stage process and later exhibits the same two-stage hematite decomposition as OreA. In order to compare the differences between thermal decomposition and the mixed mechanism, Fig. 6 relates the mass loss due to only thermal decomposition from our previous study [11], with the mixed mechanism reduction in this study for the three different atmospheres: A7.5H_2, A22.5H_2 and A37.5H_2. Considering the mass loss in reducing gas atmosphere, two distinctive stages are observed. Comparing the behaviour of the mixed reduction to the thermal decomposition, reactions can be assigned to the respective stages of the mixed reduction. The first stage for OreA is the initial reduction of hematite and the second stage the simultaneous decomposition of the dolomite phase and further iron oxide reduction. Considering OreB and OreC, the first mass loss stage is the simultaneous decomposition of the goethite phase and the reduction of hematite. The second stage is the further reduction of the iron oxides. In A7.5H_2 and A22.5H_2, all three ores reach a maximum of mass loss at a similar time, even before the set-temperature of 1773 K was reached. In A7.5H_2, the reaction saturates between 1125 and 1180 K, depending on the ore. In A22.5H_2, the reaction saturates at slightly lower temperatures, between 1095 and 1125 K. In A37.5H_2, however, the reaction seems to continue much longer and only reaches its mass loss peak between 1415 and 1440 K, depending on the ore, before the mass increases again. The mass gain phenomenon will be explained by the water-gas shift reaction (WGSR) in the following section (3.4. The influence of water-gas shift reaction).

3.4. The influence of water-gas shift reaction

The presence of hydrogen, carbon monoxide and carbon dioxide at

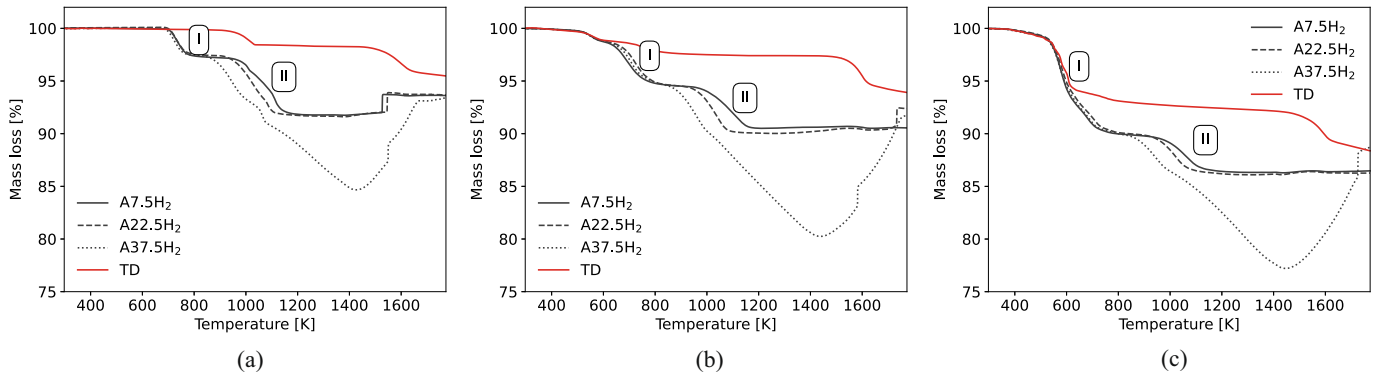

Fig. 6. Comparison of thermal decomposition (TD) [11] and mixed reduction in non-isothermal conditions for (a) OreA, (b) OreB and (c) OreC.

increasing temperatures, as investigated in this study, leads to the occurrence of the water-gas shift reaction described in (equation (9)) [42]. The water-gas shift reaction is reversible and exothermic [43].

$$H_2O(g) + CO(g) \leftrightarrow CO_2(g) + H_2(g) \quad (9)$$

Due to this reaction, the actual gas compositions present during reduction may differ from the injected gas streams and vary as a function of temperature. An important criteria to evaluate the equilibrium state of the reaction is the reaction rate constant (equation (10)).

$$K = \frac{(P_{CO_2} * P_{H_2})}{(P_{CO} * P_{H_2O})} \quad (10)$$

FactSage 7.0 [33,34] was used to investigate the temperature influence on the WGSR (Fig. 7). Up to 1100 K, the equilibrium constant is larger than 1, indicating an exothermic reaction, hence favouring the products CO_2 and H_2. Exceeding this temperature, the equilibrium shifts, and the reaction turns endothermic, favouring the development of the reactants CO and H_2O.

To further analyse the theoretical gas atmospheres in equilibrium, the Equilib module of FactSage 7.0 [33,34] was used (Fig. 8). The gas atmosphere was calculated for the volume of the reaction zone in the TGA (51 cm^3). The input streams were calculated so that the reaction chamber was completely filled with the reaction gas. The values were calculated for every 10 K.

Since this study focuses on the influence of hydrogen on the conversion degree of the ores, it is important to evaluate the actual presence of hydrogen in the system. Based on Fig. 7, the production of H_2 and CO_2 should be theoretically favoured up to around 1100 K. For all atmospheres in Fig. 8, it is shown that the hydrogen content is low at lower temperatures (< 700 K), but it steadily increases until it reaches a maximum between 863 and 943 K. The maximum concentrations are somewhat lower than the actual input streams (6.1 %, 16.2 %, and 33.0 % for A7.5H_2, A22.5H_2, and A37.5H_2, respectively). After reaching its peak, the hydrogen concentration decreases until the end temperature of calculation (1773 K). The concentrations at 1773 K are 1.7 %, 6.1 % and 22.5 % for A7.5H_2, A22.5H_2 and A37.5H_2, respectively. Based on the thermodynamics of the WGSR, the water-vapour content should show an opposite trend to hydrogen. In Fig. 8 the course of water-vapour depends on the amount of hydrogen in the input gas. Even though water-vapour is not present in the input gas stream, it increases to high levels, varying between 15 and 30 vol-% in A37.5H_2. As expected from the WGSR, CO_2 behaves opposite to the course of water-vapour and starts to decrease when the amount of water-vapour in the system increases. Even though the amount of CO_2 is still high in A7.5H_2 at 1773 K (51.5 %), it decreases to 12.8 % in A37.5H_2 at 1773 K. In A22.5H_2 and A37.5H_2, CO appears in equilibrium only from about 600 K, which is the temperature at which CO_2 begins to decrease. At 1773 K the CO content is the highest for A7.5H_2 (38.2 %). The CO content is higher in A37.5H_2 (37.5 %), compared to A22.5H_2 (33.9 %) even though the input amount is the same. This can be explained by the general lower amounts of CO_2 in the system.

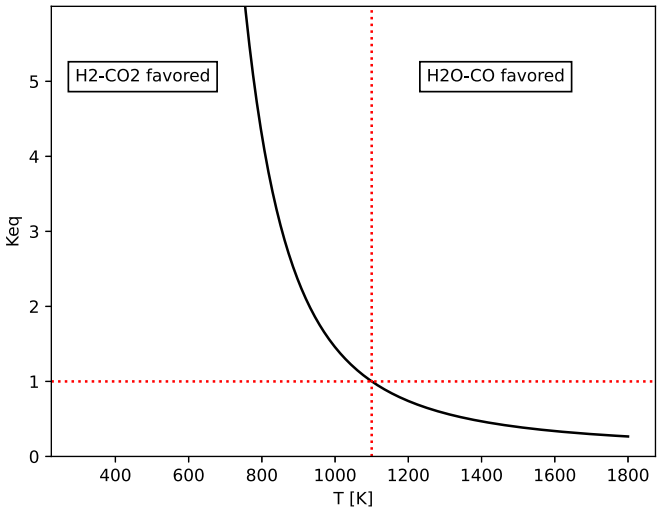

Fig. 7. Influence of temperature on water-gas shift reaction in a temperature range of 300 to 1800 K (FactSage 7.0) [33,34].

To investigate the behaviour of the gas composition during the actual experiments, the off-gas signal was measured via a Quadruple Mass Spectrometer (QMS) in all experiments. Since the input material has no significant influence on the gas composition, the results are shown only for OreB. These include the complete mass loss over the experimental time, together with the logarithmic QMS signals (in ampere) for H_2, H_2O, CO and CO_2 as presented in Fig. 9. The data is presented until the end of the isothermal holding time, since the system is cooled in argon atmosphere afterwards. The signal measured in the QMS analysis only provides semi-quantitative data. Therefore, the measured data cannot be directly translated into vol-%, as presented for the thermodynamic calculations in Fig. 8. Nevertheless, the signal measured via QMS still provides significant data on the behaviour of the different gases and how they interact with each other, and their course can be compared to the results of the thermodynamic analysis. The corresponding data for the other ores are provided in Fig.S2 and Fig.S3 of the supplementary materials.

The course of CO_2 is measured to be relatively constant during the non-isothermal and following isothermal zone and does not indicate the same constant decrease as in the FactSage calculations. In A7.5H_2, CO behaves similarly to CO_2. However, in A22.5H_2 and A37.5H_2, where the CO content is comparatively lower, CO initially decreases slightly before it increases back to its initial value. A more chaotic trend is observed for H_2 and H_2O. In all atmospheres, as expected based on the thermodynamic calculations, a strong increase in the H_2O signal during the

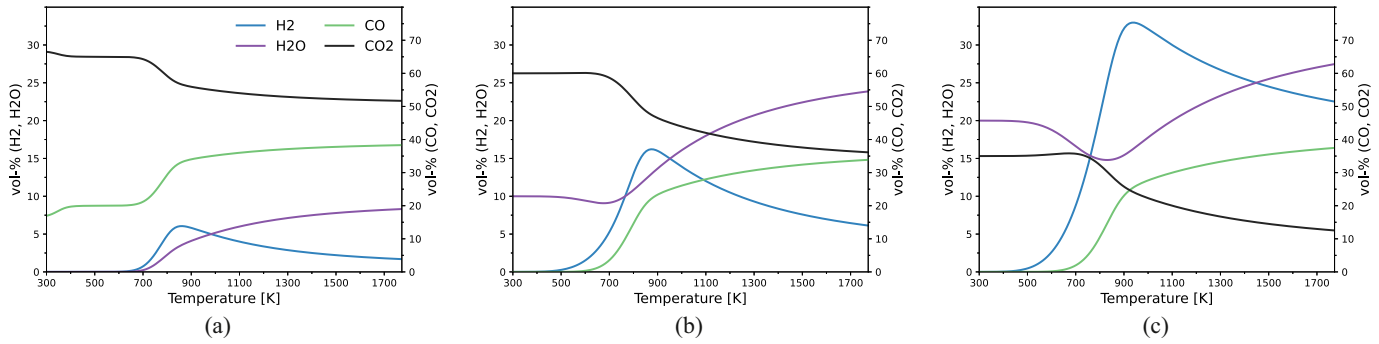

Fig. 8. Influence of water-gas shift reaction on equilibrium composition of the gas phase for (a) A7.5H_2, (b) A22.5H_2 and (c) A37.5H_2 (Fact7.0, Equilib Module [33,34]).

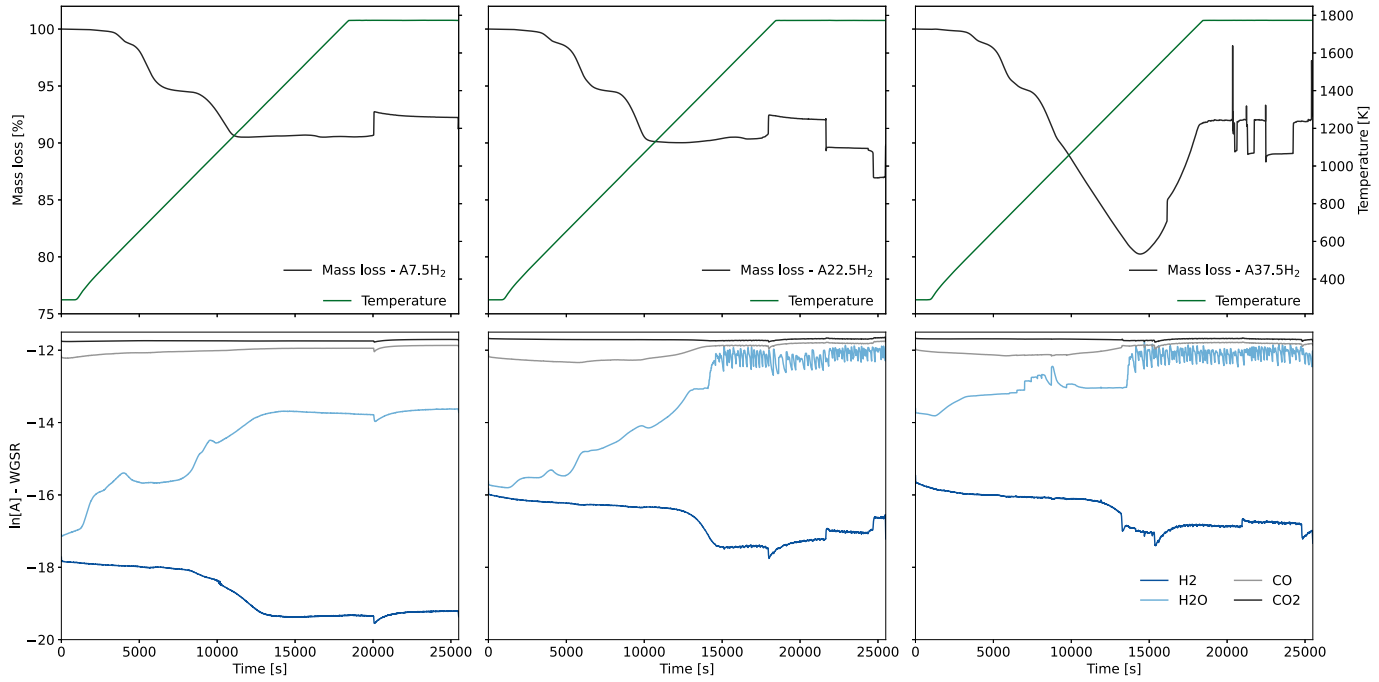

Fig. 9. QMS off-gas measurements together with mass loss for A7.5H_2, A22.5H_2 and A37.5H_2 of OreB at 1773 K.

heating stage is measured. It is important to note that the initially measured H_2O can also be emitted from the decomposing goethite phase, which was found to decompose between 436 and 918 K at a heating rate of 5 K/min [11]. During the heating phase, the hydrogen signal behaves inversely to the water-vapour. While H_2O is partly produced by the reduction of the ore (consuming H_2), most hydrogen is produced by the water-gas shift reaction. In the QMS measurement, the initial increase in H_2 as in the thermodynamic modelling is not observed. Instead a slow continuous decrease is observed with increasing temperature. The impact of the reduction by H_2 is therefore more significant at lower temperatures and decreases with the increase in temperature.

If we consider the whole mass loss in Fig. 9, also including the isothermal zone, a strange phenomenon is occurring in later stages of the experiment. During the isotherm, after the mass loss obtained in the heating zone, an increase in mass followed by a “noise” effect of fluctuating masses arises. The effect appears to be stronger for A22.5H_2 compared to A7.5H_2, apparently affected by the hydrogen increase in the atmosphere. Considering A37.5H_2, a further increase of hydrogen seems to intensify the phenomenon even more. Even though the gases are constantly fed into the system, only CO and CO_2 stay constant during the course of the experiment. For hydrogen and water-vapour, the stronger observed fluctuations are related to pressure changes in the

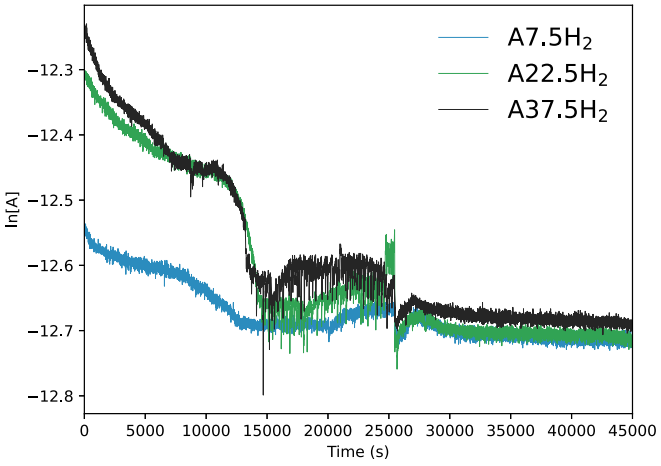

Fig. 10. Total pressure during the experiments of OreB under the reducing atmosphere of A7.5H_2, A22.5H_2 and A37.5H_2.

system. These fluctuations initiate at approximate temperatures of 1410 K for A22.5H_2 and of 1370 K for A37.5H_2, indicating the on-set temperatures of strong reactions of the WGSR in the respective atmospheres. Fig. 10 shows the total pressure profile measured in the system during the experiments of OreB for A7.5H_2, A22.5H_2 and A37.5H_2. During the heating zone, the total pressure profile follows the course of hydrogen gas, indicating that hydrogen consumption by reduction and the water-gas shift reaction causes a decrease in total system pressure. During the isotherm, the total pressure shows similar fluctuating behaviour compared to the H_2O signal and is similar in course to the hydrogen and mass loss. Based on this, the fluctuating mass loss during the isothermal zone is most likely explained by the total pressure changes in the system. This also explains the observed mass gain phenomenon mentioned in Fig. 2 and Fig. 6. To prove the fact that this doesn't affect the mass loss signal during the reaction in the non-isothermal zone, experiments without the addition of input material under A7.5H_2 and A37.5H_2 atmosphere were conducted. The results of these mass losses can be found in the supplementary materials, in Fig.S4. Also in these runs, the same "noise" effect occurs during the isothermal zone, but does not influence the mass loss observed for the experiments during the heating zone.

3.5. Non-isothermal iron ore conversion

The non-isothermal reduction approach presents the challenge that, in addition to the reduction of Fe_2O_3, other components such as FeOOH and $CaMg(CO_3)_2$ also undergo thermal decomposition. A lot of literature is available on the thermal decomposition of goethite and hematite, as well as of the gas-solid reduction [11,13,25–32]. However, as mentioned before, these studies do not observe the gas-solid reduction and thermal decomposition as simultaneous mechanisms. Due to the co-occurrence of the gas reduction of the hematite phase and the thermal decomposition of the goethite and dolomite phases in this study, the individual mass loss stages cannot be assigned to a specific reaction. As a result, the calculation of the conversion factor must be adjusted, as shown in equation (11).

$$\alpha = \frac{m_0 - m_t}{m_0 - \left(m_0 - m_0 * \left(\frac{X_{H_2O}}{100} + \frac{X_{CO_2}}{100} + \frac{X_{O_{Fe_2O_3 \rightarrow FeO}}}{100}\right)\right)} \quad (11)$$

Where m_0 is the initial mass of the sample (mg), m_t is the mass at time t (mg), X_{H_2O} is the amount of crystal water measured in the sample (wt %), X_{CO_2} is the amount of CO_2 measured in the sample (wt%) and $X_{O_{Fe_2O_3 \rightarrow FeO}}$ is the theoretical amount of oxygen lost, considering a reduction from Fe_2O_3 to FeO.

This revised representation of the conversion factor accounts for the complete conversion of all phases that would be reduced during ore decomposition, contributing to the overall mass loss of the sample. Meaning, a conversion factor of 1 would describe the complete decomposition of dolomite (OreA) or goethite (OreB & OreC) combined with the reduction of hematite to wustite. Therefore, the newly defined conversion degree does not reflect the reduction of the iron phase anymore and is solely used as a parameter, describing the complete process. The conversion factors for the non-isothermal gas reduction of the three ores in A7.5H_2 and A22.5H_2, calculated based on equation (11), are presented in Fig. 11. The high mass loss observed for A37.5H_2 in Fig. 6 would lead to a conversion significantly larger than 1, which is unlikely to occur, as these numbers would imply the presence of iron. Since the reduction under isothermal conditions in the A37.5H_2 atmosphere also did not lead to a conversion degree larger than 1, it is unlikely to achieve it under non-isothermal conditions. The authors suggest that the conversion reaches a similar level compared to A7.5H_2 and A22.5H_2 and the following increase can be explained by the pressure variance due to the water-gas shift reaction, as explained in the previous section. Therefore, the results of A37.5H_2 are excluded from this analysis of the conversion degree.

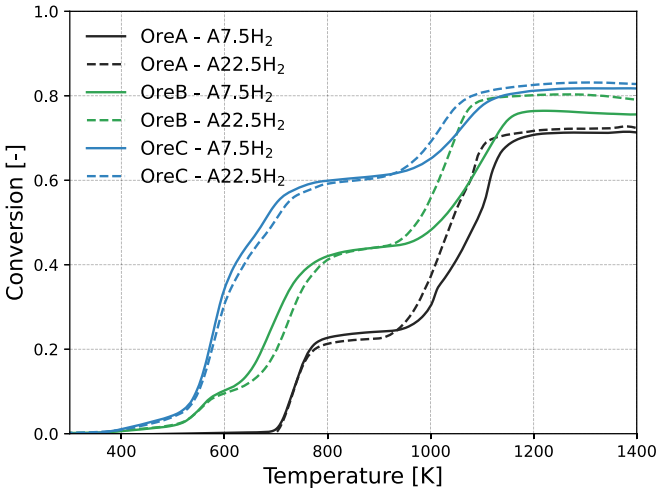

Fig. 11. Conversion factors for OreA, OreB and OreC in the atmospheres A7.5H_2 and A22.5H_2.

Even though the initial conversion seems similar for all atmospheres of the same ores (OreA: $\alpha < \sim 0.2$, OreB: $\alpha < \sim 0.4$, OreC: $\alpha < \sim 0.6$), higher conversion is achieved in the second conversion stage at lower temperatures with increasing hydrogen-levels. This phenomenon can be explained by the hematite reduction becoming the dominant conversion mechanism after the decomposition of other components, and this stage is more influenced by the enrichment of hydrogen in the reducing gas. For all three ores the influence of the increasing H_2-levels on the final conversion value is marginal. For OreA the conversion increases from approximately 71 to 72 %, for OreB from 76 to 80 % and for OreC from 82 to 83 %, for A7.5H_2 and A22.5H_2 respectively. Since for all ores it is expected that all possible thermal decomposition reactions are completed during the reduction and the only limiting reaction is the conversion from hematite to wustite, the final conversion degrees of the ores are comparable. A clear difference in the final conversion between the three ores is visible. It seems that an increasing amount of goethite in the sample leads to an increase in total conversion, as lowest conversion is observed for OreA (no crystal water) and highest for OreC (6.05-% crystal water). An explanation for this can be that the decomposition of goethite leads to a more fine-grained and porous structure and, therefore, to a more reactive hematite phase compared to the hematite in the virgin material. Li et al. [44] found that the heating and dehydration of goethite ores generate cracks and result in a more porous structure of the ore. Unfortunately, since this transformation occurs in the initial stages of the reduction in our experiments, it is not possible to verify this influence with microscopical analysis. In our previous study [11], as well as in other studies such as by Xing et al. [31] and Dilmaç [30], the Coats-Redfern Method [45] was applied to obtain kinetic parameters of hematite reduction and thermal decomposition in non-isothermal conditions at a single constant heating rate. However, the Coats-Redfern method is not applicable here due to the multiple simultaneous reactions that cannot be easily separated. Therefore, this study will not determine the kinetic parameters of the non-isothermal gas reduction of the different ores and will leave this to future studies, along with the morphological study of the previous proposed goethite thermal decomposition.

4. Conclusions

- In the isothermal experiments, an increase in H_2 in the reducing gas atmosphere enhances the conversion to wustite within a temperature range of 1673–1773 K. Lowering the PCR from 60 % to 40 % and, therefore, increasing the H_2 level, further improves the conversion. A higher H_2 content not only increases the limit of conversion but also

decreases the time after which the conversion saturates. In A7.5H_2 the conversion saturates between 502 and 794 s, in A22.5H_2 between 375 and 583 s and in A37.5H_2 between 206 and 297 s, depending on the temperature. Faster conversion is achieved at higher temperatures.

- Microscopical observations and model fitting based on the shrinking core model of the isothermal experiments indicate that the diffusion of the reacting gas through the developing product layer is the rate-determining mechanism. The activation energy decreases from 77.60 to 69.12 kJ/mol with an increase in H_2 in the same PCR, but increases to 79.91 kJ/mol with a decrease in PCR from 60 to 40 % in a temperature range of 1673–1773 K.
- Comparing the mass loss of the non-isothermal gas reduction to the isolated thermal decomposition, the initial reduction of hematite in OreA starts before the reduction proceeds simultaneously with dolomite decomposition. For OreB and OreC a first significant mass loss curve describes the simultaneous initial reduction of hematite together with goethite thermal decomposition, whereas only iron oxide reduction is observed at later stages.
- During the heating stage of the non-isothermal experiments, the water-gas shift reaction (WGSR) is clearly observable. The partial pressure of water-vapour in the gas atmosphere increases continuously, while that of H_2 decreases. During the later isotherm, the reactions of the WGSR lead to pressure changes in the system, influencing the mass loss data.
- In the non-isothermal experiments, the influence of ore mineralogy on the total conversion is stronger than the influence of H_2-enrichment in the atmosphere. Higher conversion is achieved with increasing goethite content in the ores: α_{OreA} (71–72 %) < α_{OreB} (76–80 %) < α_{OreC} (82–83 %). However, as in the isothermal experiments, the increase of H_2 in the atmosphere increases the speed of reduction and leads to conversion at lower temperatures. Overall, there is no significant difference on the final conversion achieved in the non-isothermal experiments (76–80 %) compared to the isothermal experiments (73–81 %) of OreB.

CRediT authorship contribution statement

Philipp Leerhoff: Writing – review & editing, Writing – original draft, Visualization, Validation, Software, Methodology, Investigation, Formal analysis, Data curation, Conceptualization. **Johannes C. Brouwer:** Validation, Investigation. **Christiaan Zeilstra:** Writing – review & editing, Supervision, Resources, Project administration, Funding acquisition. **Koen Meijer:** Writing – review & editing, Supervision. **Jan van der Stel:** Writing – review & editing, Supervision. **Shoshan T. Abrahami:** Writing – review & editing, Supervision. **Neslihan Dogan:** Writing – review & editing, Supervision. **Yongxiang Yang:** Writing – review & editing, Supervision, Resources, Project administration, Funding acquisition.

Funding

This research was carried out under project number T20009 in the framework of the Research Program of the Materials innovation institute (M2i) (www.m2i.nl) supported by the Dutch government.

Declaration of competing interest

The authors declare that they have no known competing financial interests or personal relationships that could have appeared to influence the work reported in this paper.

Acknowledgments

Ruud Hendrikx and Richard Huizenga at the Department of Materials Science and Engineering of the Delft University of Technology are acknowledged for the XRD analysis.

Appendix A. Supplementary data

Supplementary data to this article can be found online at https://doi.org/10.1016/j.powtec.2025.121570.

Data availability

Data will be made available on request.

References

[1] worldsteel Association, Climate Change and the Production of iron and Steel, Brussels, 2021.
[2] worldsteel association, Sustainable Performance of Steel Industry 2003–2021, Brussels, 2022.
[3] M. Naito, K. Takeda, Y. Matsui, Ironmaking Technology for the Last 100 years: deployment to advanced technologies from introduction of technological know-how, and evolution to next-generation process, ISIJ Int. 55 (2015) 7–35, https://doi.org/10.2355/isijinternational.55.7.
[4] S. Seetharaman, R. Guthrie, A. McLean, S. Seetharaman, H. Yong Sohn, Treatise on process metallurgy, in: Industrial Processes, 2nd ed. vol. 3, Elsevier Ltd., 2024.
[5] K. Meijer, C. Guenther, R.J. Dry, HIsarna Pilot Plant Project, 2011.
[6] S. Santos, K. Meijer, J. Van Der Stel, P. Broersen, J. Monteiro, P. Van Os, CO2 capture in combination with the HIsarna process, in: METEC & 4th ESTAD 2019, European Steel Technology and Application Days, Duesseldorf, 2019.
[7] K. Meijer, C. Zeilstra, C. Teerhuis, M. Ouwehand, J. van der Stel, Developments in alternative ironmaking, Trans. Indian Inst. Metals 66 (2013) 475–481, https://doi.org/10.1007/s12666-013-0309-z.
[8] Z. Yan, T.T. Htet, J. Hage, K. Meijer, Z. Li, HIsarna process simulation model: using FactSage with macro facility, Metall. Mater. Trans. B 54 (2023) 868–879, https://doi.org/10.1007/s11663-023-02732-5.
[9] Y. Yang, K. Raipala, L. Holappa, Ironmaking, in: Treatise on Process Metallurgy, Elsevier Ltd., 2014, pp. 2–88, https://doi.org/10.1016/B978-0-08-096988-6.00017-1.
[10] A.K. Biwas, Principles of Blast Furnace Ironmaking : Theory and Practice, Brisbane, 1981.
[11] P. Leerhoff, J.C. Brouwer, A.M. Armaki, C. Zeilstra, K. Meijer, J. van der Stel, S. T. Abrahami, N. Dogan, Y. Yang, Characterisation of varying Iron ores and their thermal decomposition kinetics under HIsarna ironmaking conditions, Metals (Basel) 14 (2024) 1271, https://doi.org/10.3390/met14111271.
[12] Y. Qu, Y. Yang, Z. Zou, C. Zeilstra, K. Meijer, R. Boom, Thermal decomposition behaviour of fine iron ore particles, ISIJ Int. 54 (2014) 2196–2205, https://doi.org/10.2355/isijinternational.54.2196.
[13] Z. Chen, C. Zeilstra, J. Van Der Stel, J. Sietsma, Y. Yang, Thermal decomposition reaction kinetics of hematite ore, ISIJ Int. 60 (2020) 65–72, https://doi.org/10.2355/isijinternational.ISIJINT-2019-129.
[14] P.C. Cavaliere, Hydrogen assisted direct reduction of Iron oxides, Springer International Publishing (2022), https://doi.org/10.1007/978-3-030-98056-6.
[15] A.O. Zhang, B.J. Monaghan, R.J. Longbottom, M. Nusheh, C.W. Bumby, Reduction kinetics of oxidized New Zealand Ironsand pellets in H2 at temperatures up to 1443 K, Metall. Mater. Trans. B 51 (2020) 492–504, https://doi.org/10.1007/s11663-020-01790-3.
[16] I. Sohn, S.M. Jung, Effect of metal additions to the reduction of Iron oxide composite pellets with hydrogen at moderate temperatures, Steel Res Int 82 (2011) 1345–1354, https://doi.org/10.1002/srin.201100144.
[17] H. Zuo, C. Wang, J. Dong, K. Jiao, R. Xu, Reduction kinetics of iron oxide pellets with H2 and CO mixtures, Int. J. Miner. Metall. Mater. 22 (2015) 688–696, https://doi.org/10.1007/s12613-015-1123-x.
[18] I.-J. Moon, C.-H. Rhee, D.-J. Min, Reduction of hematite compacts by H2-CO gas mixtures, Steel Research 69 (1998) 302–306, https://doi.org/10.1002/srin.199805555.
[19] E. Kawasaki, J. Sanscrainte, T.J. Walsh, Kinetics of reduction of iron oxide with carbon monoxide and hydrogen, A.I.Ch.E. J. 8 (1962) 48–52.
[20] M. Kazemi, M. Saffari Pour, D. Sichen, Experimental and modeling study on reduction of hematite pellets by hydrogen gas, Metall. Mater. Trans. B Process Metall. Mater. Process. Sci. 48 (2017) 1114–1122, https://doi.org/10.1007/s11663-016-0895-3.
[21] I. Sohn, R.J. Fruehan, The reduction of Iron oxides by volatiles in a rotary hearth furnace process: part I. The role and kinetics of volatile reduction, Metall. Mater. Trans. B 36 (2005) 605–612.
[22] D. Spreitzer, J. Schenk, Iron ore reduction by hydrogen using a laboratory scale fluidized bed reactor: kinetic investigation—experimental setup and method for determination, Metall. Mater. Trans. B 50 (2019) 2471–2484, https://doi.org/10.1007/s11663-019-01650-9.
[23] K. Piotrowski, K. Mondal, H. Lorethova, L. Stonawski, T. Szymański, T. Wiltowski, Effect of gas composition on the kinetics of iron oxide reduction in a hydrogen production process, Int. J. Hydrogen Energy 30 (2005) 1543–1554, https://doi.org/10.1016/J.IJHYDENE.2004.10.013.
[24] D. Spreitzer, J. Schenk, Reduction of Iron oxides with hydrogen—a review, Steel Res Int 90 (2019) 1900108, https://doi.org/10.1002/srin.201900108.

[25] P.C. Beuria, S.K. Biswal, B.K. Mishra, G.G. Roy, Study on kinetics of thermal decomposition of low LOI goethetic hematite iron ore, Int. J. Min. Sci. Technol. 27 (2017) 1031–1036, https://doi.org/10.1016/j.ijmst.2017.06.018.
[26] P. Pourghahramani, E. Forssberg, Reduction kinetics of mechanically activated hematite concentrate with hydrogen gas using nonisothermal methods, Thermochim. Acta 454 (2007) 69–77, https://doi.org/10.1016/j.tca.2006.12.023.
[27] B. Lyu, G. Wang, F. Yang, H. Zuo, Q. Xue, J. Wang, Kinetic analysis of isothermal and non-isothermal reduction of Iron ore fines in hydrogen atmosphere, Metals (Basel) 12 (2022) 1754, https://doi.org/10.3390/met12101754.
[28] A. Hammam, Y. Li, H. Nie, L. Zan, W. Ding, Y. Ge, M. Li, M. Omran, Y. Yu, Isothermal and non-isothermal reduction behaviors of Iron ore compacts in pure hydrogen atmosphere and kinetic analysis, Min Metall Explor 38 (2021) 81–93, https://doi.org/10.1007/s42461-020-00317-3.
[29] Y. Sun, Y. Han, X. Wei, P. Gao, Non-isothermal reduction kinetics of oolitic iron ore in ore/coal mixture, J. Therm. Anal. Calorim. 123 (2016) 703–715, https://doi.org/10.1007/s10973-015-4863-y.
[30] N. Dilmaç, Isothermal and non-isothermal reduction kinetics of iron ore oxygen carrier by CO: Modelistic and model-free approaches, Fuel 296 (2021) 120707, https://doi.org/10.1016/j.fuel.2021.120707.
[31] L. Xing, Y. Qu, C. Wang, L. Shao, Z. Zou, W. Song, Kinetic study on thermal decomposition behavior of hematite ore fines at high temperature, Metall. Mater. Trans. B 51 (2020) 395–406, https://doi.org/10.1007/s11663-019-01747-1.
[32] A. Ammasi, Effect of heating rate on decomposition temperature of goethite ore, Trans. Indian Inst. Metals 73 (2020) 93–98, https://doi.org/10.1007/s12666-019-01806-w.
[33] CRCT, ThermFact Inc, FactSage, Equilib Module, GTT-Technologies, 2015.
[34] CRCT, ThermFact Inc, FactPS Database, GTT-Technologies, 2015.
[35] O. Levenspiel, Fluid-particle reactions: Kinetics, in: Chemical Reaction Engineering, 3rd ed, John Wiley & Sons, 1999.
[36] Y. Luo, Y. Wu, Comment on “effects of particle size and coating on decomposition of alumina-extracted residue from high-alumina fly ash”: proposition of the shrinking cylinder model, J. Hazard. Mater. 401 (2021), https://doi.org/10.1016/j.jhazmat.2020.123818.
[37] Y.H. Han, J.S. Wang, R.Z. Lan, L.T. Wang, X.J. Zuo, Q.G. Xue, Kinetic analysis of iron oxide reduction in top gas recycling oxygen blast furnace, Ironmaking Steelmaking 39 (2012) 313–317, https://doi.org/10.1179/1743281211Y.0000000058.
[38] L.Y. Xing, Z.S. Zou, Y.X. Qu, L. Shao, J.Q. Zou, Gas–solid reduction behavior of in-flight fine hematite ore particles by hydrogen, Steel Res. Int. 90 (2019) 1–10, https://doi.org/10.1002/srin.201800311.
[39] Y. Qu, Y. Yang, Z. Zou, C. Zeilstra, K. Meijer, R. Boom, Reduction kinetics of fine hematite ore particles with a high temperature drop tube furnace, ISIJ Int. 55 (2015) 952–960, https://doi.org/10.2355/isijinternational.55.952.
[40] M. Bahgat, M.H. Khedr, Reduction kinetics, magnetic behavior and morphological changes during reduction of magnetite single crystal, Mater. Sci. Eng. B 138 (2007) 251–258, https://doi.org/10.1016/j.mseb.2007.01.029.
[41] H. Chen, Z. Zheng, W. Shi, Investigation on the kinetics of Iron ore fines reduction by CO in a Micro-fluidized bed, Procedia Eng 102 (2015) 1726–1735, https://doi.org/10.1016/j.proeng.2015.01.308.
[42] G.K. Reddy, P.G., Smirniotis, in: Introduction about WGS Reaction, in: Water Gas Shift Reaction, Elsevier, 2015, pp. 1–20, https://doi.org/10.1016/B978-0-12-420154-5.00001-2.
[43] D.S. Newsome, The water-gas shift reaction, Catal. Rev. 21 (1980) 275–318, https://doi.org/10.1080/03602458008067535.
[44] H. Li, D.J. Pinson, P. Zulli, L. Lu, R.J. Longbottom, S.J. Chew, B.J. Monaghan, G. Zhang, Interaction between mineral phases in a Goethitic Iron ore and fluxing materials during sintering, Metall. Mater. Trans. B 52 (2021) 996–1011, https://doi.org/10.1007/s11663-021-02072-2.
[45] A.W. Coats, J.P. Redfern, Kinetic parameters from thermogravimetric data, Nature 201 (1964) 68–69, https://doi.org/10.1038/201068a0.